Asian Journal of Chemistry; Vol. 34, No. 5 (2022), 1206-1212

ASIAN JOURNAL OF CHEMISTRY

https://doi.org/10.14233/ajchem.2022.23739

Efficiency Enhancement of Dye Sensitized Solar Cell Using Composite P25-TiO_2/Carbon Nanotubes Photoanode with Platinum Counter Electrode

SAMAA S. MAHMOOD[1], FALAH H. HUSSIEN[2,*] and ABBAS J. ATIYAH[1]

[1]Department of Chemistry, University of Babylon, College of Science, Babylon, Iraq
[2]Department of Chemistry, University of Babylon, College of Pharmacy, Babylon, Iraq

*Corresponding author: E-mail: abohasan_hilla@yahoo.com

Received: 22 January 2022; *Accepted*: 11 February 2022; *Published online*: 20 April 2022; AJC-20773

Present study includes enhancing the efficiency of the prepared dye sensitized solar cell (DSSC) by using Degussa (Evonik) P25 with carbon nanotubes (CNTs) composites as the photoanode electrode instead of using TiO_2 alone. Platinum was used as the counter electrode with the use of natural pomegranate dye and KI/I_2 as electrolyte solution. The morphology of the prepared composites were characterized using X-ray diffraction (XRD), Raman spectroscopy, scanning electron spectroscopy (SEM) and UV-visible diffuse reflectance spectra for all ratios prepared from P25/CNTs composites, The results showed that the CNTs dopant were incorporated into interstitial position of the P25 lattice nanoribbons with diameter of (30-75) nm and length of few micrometers. The calculated optical band gap for P25 and P25/CNTs in ratios 1:2.5% were 3.22 eV and 3.00, respectively. These modified properties of the P25/CNTs composites showed an important effect on the conversion efficiency of the assembled dye sensitized solar cells, where the efficiency of the P25 and P25/CNTs composites was 2.962% and 3.679%, respectively. This indicates that the efficiency of the DSSCs was increased relatively when using P25/CNTs composite instead of P25 alone as a photoanode when the other components of the cell were applied under the same preparation and fabrication conditions for the investigated DSSCs.

Keywords: Dye sensitized solar cell, Degussa (P25-TiO_2), P25/CNTs nanocomposites, Pt counter electrode.

INTRODUCTION

Although the dye-sensitized solar cells (DSSCs) have been known for a long time for their conversion efficiencies have remained low. Following the discovery of high efficiencies of DSSC by O'Regan & Grätzel in the early 1990s [1], this form of solar cell is being further developed with the goal of producing wide-area and cheap-cost solar cells [2]. A solar cell uses a semiconductor to directly convert solar energy into electrical power. Due to their ease of manufacture, high efficiency of power conversion and low cost DSSCs have recently been suggested as an appealing candidate for the third solar cell generation. Due to their high conversion efficiency, DSSCs are an effective technology when compared to other organic cells. The DSSC system's photovoltaic performance is influenced by a number of factors, including the sensitizer's absorption range, molar absorption coefficient, high performance electrolyte for dye regeneration, sheet resistance of conducting transparent substrates and photochemically stable semiconductor materials [3-5]. Much of the current research is focused on increasing the efficiency of DSSC by substituting typical ruthenium dyes with organic dyes and producing photoanodes using other metal oxide semi-conductors such as zinc oxide (ZnO), titanium dioxide (TiO_2) and tin dioxide (SnO_2) [6-8].

Titanium dioxide is one of the most studied photo anode materials for DSSCs due to its high chemical and thermal stability, low cost, high refractive index and favourable conduction band edges for efficient electron injection to many sensitizers [5,9,10]. The physical and structural properties of TiO_2, including crystal size, morphology, phase composition, porosity, thickness of TiO_2 layer and specific surface area, strongly depend on the physical and structural properties of TiO_2 to achieve strong light scattering capacity, dye loading ability, electron hole pair separation efficiency, electron transport and diffusion of electrolyte [11-13]. The first DSSC device was made of TiO_2 nanoparticles, which have a large surface area for fast

dye loading but are inefficient due to unpredictable electron-pathways and dead ends that impede electron transport [14]. When compared to nanoparticles, one-dimensional (1D) nanostructures like nanorods [15], nanowires [16] and nanotubes [17] have been shown to provide improved directed paths for electrons to reach the conductive substrates. These 1D nanostructures reduce the number of dead ends in electron transport [18].

The TiO_2 Degussa P25 is one of the most commonly used commercial TiO_2 materials for photocatalytic oxidation applications and suitable for the fabrication of effective dye-sensitized solar cells. This industrial catalyst is made up of 80% anatase and 20% rutile, with a surface area of 50 $m^2 g^{-1}$ and a particle size of 21 nm [19,20]. The current study involves the fabrication of dye sensitized solar cells with composites of P25 and CNTs in different ratios and investigated as the active electrode. Conversion efficiency of the assembled dye sensitized solar cells with photoanode of P25 and P25/CNTs composites is also investigated.

EXPERIMENTAL

Titanium oxide nanoparticles P25-TiO_2 (Degussa) (20 nm) (95%, Evonik, Germany), Triton X-100 (Sigma-Aldrich, USA), hexachloroplatinic acid ($H_2PtCl_6 \cdot 6H_2O$, 99%, Evonik, Germany), isopropanol (99%, BDH), nitric acid (73%, CDH, India), acetone (99%, S.D. Fine-chem. Ltd., India) were procured for this study.

Synthesis of carbon nanotubes using flame fragment deposition method: In flame fragment deposition (FFD) method, using a homemade chamber instrument was used for the synthesis of carbon nanotubes (CNTs) using LPG as a carbon source [21,22]. Schematic description of this unit is shown in Fig. 1.

Synthesis of TiO_2/CNTs composites: A simple evaporation and drying process was used to create different ratios of titanium dioxide nanoparticles P25/CNTs composites. To make P25/CNTs composite, 10 mg CNTs were dispersed in 150 mL of deionized distilled water and sonicated for 15 min. Titanium dioxide powder was then added to the CNTs suspension while stirring continuously. The suspension containing CNTs and P25 particles was then sonicated for 10 min before being heated to 80 ºC to accelerate the water evaporation. The composite was then dried overnight in an oven at 104 ºC to prevent the CNTs from oxidizing. Different composites were prepared by varying the P25 and CNTs ratios. The mass ratios were as follows: 1:0.01, 1:0.025 and 1:0.05.

Fabrication of dye sensitized solar cells (DSSCs): The prepared photoanodes and counter electrodes were assembled into a sandwich DSSCs configuration, with an electrolyte drop

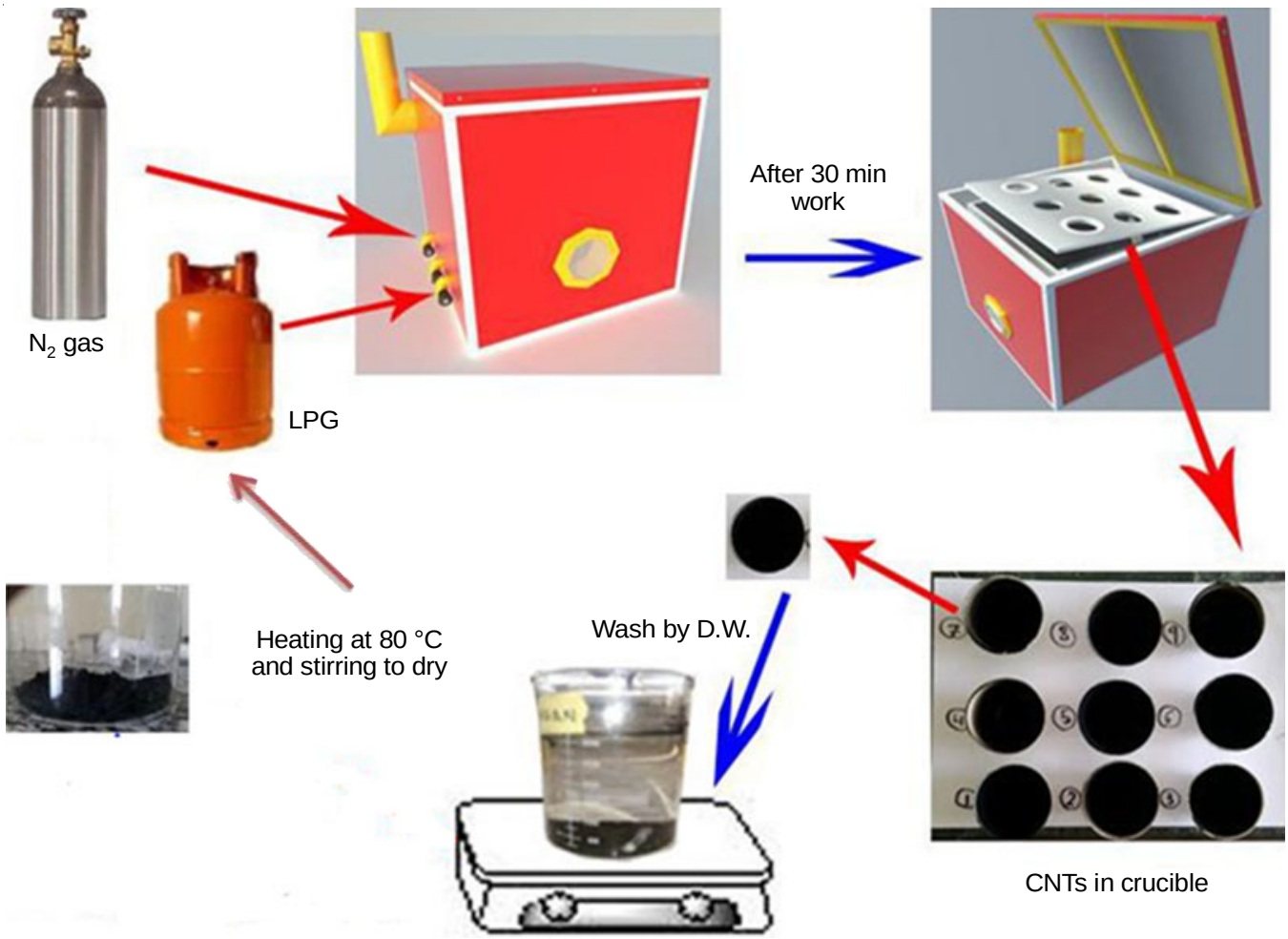

Fig. 1. Schematic diagram of the steps used by the flame fragmentations deposition instrument (FFD) to synthesize CNTs

filling the internal space. Using a Keithly 2400 source meter and under intensity light of 34 mW cm^{-2} was used. The photovoltaic performances of the prepared DSSCs, including the open-circuit voltage (V_{oc}), short-circuit current density (J_{sc}), fill factor (FF) and power conversion efficiency (η) were estimated.

Extraction of natural dyes: In current study, the used dye in fabrication of DSSCs was extracted from pomegranate fruit seeds. Extraction process was performed by collecting the pomegranate fruits from local market at Hilla city, Babylon Governorate, Iraq. The collected seeds were washed with deionized water, squeezed and then filtered through laboratory filter papers to remove the solids. The filtrate was centrifuged carefully. The deposits were then discarded and the obtained filtrate was taken. The obtained extract then kept in the dark in the refrigerator at 4 ºC [23].

Fabrication of working electrodes: The fluoride tin oxide (FTO) glass slides were cleaned carefully by washing with isopropanol for several times, followed by acetone and then finally with deionized distilled water and dried at hot air. To fabricate DSSCs, the photoanode material was used as electrodes, including P25-TiO_2 and its different composites with CNTs. For each case, FTO substrates were coated with a paste from its photoanode materials using 0.2 g. For each, 0.4 mL (0.1 M) HNO_3 and one drop of Triton X-100 ($C_{34}H_{62}O_{11}$ *m.w*. 646.87). The prepared paste was applied to FTO-glass substrates with using the glass motor to brush the material on the glass to obtain a very thin and symmetrical thickness. These samples were dried for 10 min at 80 ºC. Finally, the prepared samples were annealed for 2 h at 450 ºC before being immersed in a pomegranate dye solution for 24 h in the dark to prevent the photodegradation of dye. In order to remove the non-adsorbed dye molecules, the surface of photoanode materials was washed with ethanol carefully [24,25].

Preparation of counter electrode (CE): The FTO glass slides were thoroughly cleaned with isopropanol for 5 min, followed by acetone for another 5 min. Finally, all the cleaned substrates were deionized washed and dried. To prepare the solar cell, the cathode electrode was used, the platinum electrode being the most expensive. To make the Pt counter electrode, the hexachloroplatinic acid (H_2PtCl_6) was dropped onto the surface of FTO glass and kept for it to dry and sintered at 450 ºC in a burning furnace for 0.5 h [25].

Preparation of redox electrolyte: Between two prepared electrodes, a drop of (0.1 M) iodine solution was added and shaked until the iodine was completely dissolved and kept in the solution in an opaque bottle [26]. The counter electrode was then placed on the working electrode and the solution was kept in an opaque bottle under such conditions that the solution does not leak out of the specified area in cell.

RESULTS AND DISCUSSION

XRD of synthesized P25/CNTs composites: Fig. 2 show the XRD patterns of P25 and P25/CNTs composites generated with the various ratios (w/w) of synthesized CNTs. The P25/CNT composite catalysts have XRD patterns that are extremely close to TiO_2. The XRD pattern of P25 where several

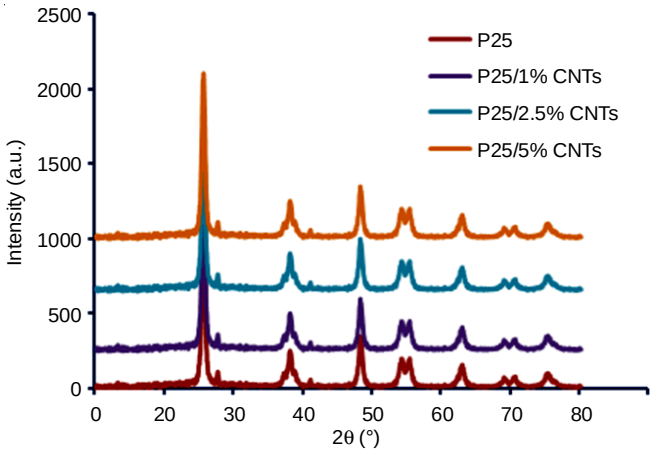

Fig. 2. XRD patterns for P25 and its composites with CNTs

characteristic peaks at 2θ = 25.5º, 27.5º, 36.5º, 37.97º, 40.9º, 48.0º, 54.0º, 55.2º, 62.8º, 68.8º, 70.17º and 75.05º for A(101), R(110), A(103), A(004), R(111), A(200), A(106), A(211), A(204), A(116), A(220) and A(215) diffractions are considered, respectively (A: anatase and R: rutile). According to it, both anatase and rutile crystallites are confirmed in P25 structure but no brukite phase is observed. If the characteristic peaks of P25 alone is compared with P25/CNTs composites (Fig. 2), it is easily understood for ratio composites from 1% to 5% CNTs, the crystallite diameters of the composite catalysts decrease steadily as the ratios of CNTs increase. With the presence of CNTs in P25, these peaks will be less strong and wider [27]. The diffraction peaks of carbon nanotubes were not clearly visible, most likely due to the composites being obscured by the much more powerful peak for the high P25 ratio or the low carbon nanotube loading amount. From the XRD data, the average crystallite size of the synthesized samples was determined using Scherrer's equation [28]:

$$d = \frac{K\lambda}{\beta\cos\theta} \quad (1)$$

where d is the crystallite size, k is a constant (0.9), λ is the wavelength of X-ray (Cu*K*α), β is the half-peak width in radians and θ is the Bragg's diffraction angle in degree. Table-1 show Values of angels of diffraction 2θ, *d*-spacing, intensities and average crystalline size of the P25 and its composites with synthesized CNTs.

Raman spectroscopy: The pure P25 in the region 100-800 cm^{-1} in the Raman spectra (Fig. 3) confirmed the presence of P25. The P25 spectrum reveals the presence of five distinct Raman lines at 130.9 cm^{-1} (E_g), 160.0 cm^{-1} (E_g), 378.9 cm^{-1} (B_{1g}), 597.8 cm^{-1} ($A_{1g} \rightarrow B_{1g}$) and 622.9 cm^{-1} (E_g), which correspond to the E_g, E_g, B_{1g}, $A_{1g} \rightarrow B_{1g}$ and E_g Raman active fundamentals of TiO_2. The E_g and A_{1g} modes of the rutile phase were detected at 438 and 599.6 cm^{-1}, respectively. The spectra measured for this sample (Fig. 3) clearly confirms the presence of both TiO_2 crystalline phases for P25, since it comprises all of the distinctive bands related to the anatase and rutile phases. All Raman bands for P25 were the same as for P25/CNT composites, with the exception of the P25 Raman bands at 150 cm^{-1}. Moreover, among the Raman bands for P25 and CNTs, the P25

TABLE-1
VALUES OF ANGELS OF DIFFRACTION 2θ, d-SPACING, INTENSITIES AND AVERAGE CRYSTALLINE SIZE OF THE P25 AND ITS COMPOSITES WITH SYNTHESIZED CNTs

Sample	2θ (°)	d (Å)	Intensity (a.u)	Average crystalline size (nm)	Sample	2θ (°)	d (Å)	Intensity (a.u)	Average crystalline size (nm)
P25	25.525	7.952767	1041.013	41.68045	P25 + 2.5% CNTs	25.525	7.952767	1274.245	44.46
	37.975	9.534813	247.1919			37.875	11.2348	238.7854	
	48.175	2.02332	302.7762			48.075	7.341419	315.7089	
	54.075	1.900411	205.4946			54.075	1.900411	204.5731	
	54.275	1.954692	182.7538			54.225	1.93929	194.8584	
	62.825	19.6765	163.9566			62.575	7.67487	145.9932	
	68.825	9.145161	71.1557			68.675	6.411245	57.9247	
	69.125	10.69378	54.6405			70.075	3.45659	59.1	
	75.075	9.61204	90.750			74.875	5.52064	82.00	
	75.175	11.343	94.7695			75.275	11.343	87.8026	
P25 + 1% CNTs	25.525	7.952767	1103.588	48.21712	P25 + 5% CNTs	25.252	7.952767	970.8537	40.26903
	37.925	11.2348	235.9039			37.925	11.2348	221.7239	
	48.175	2.02332	348.9624			48.125	2.00253	281.4974	
	54.125	1.912217	198.874			54.175	1.925155	215.2631	
	54.270	1.93929	183.6722			54.125	1.912217	150.997	
	62.825	10.1162	155.1158			62.775	10.1162	132.706	
	68.875	9.145161	62.9633			68.775	9.145161	51.9174	
	70.275	2.95592	73.5098			69.175	12.89292	65.6747	
	74.975	6.63023	88.7903			75.075	9.61204	77.6892	
	75.325	9.61204	91.8664			75.425	9.509354	81.4908	

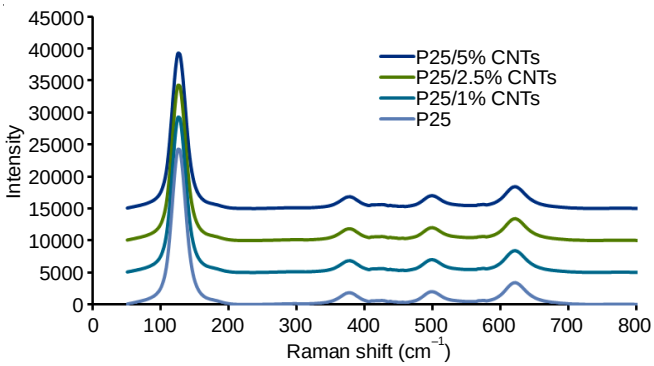

Fig. 3. Raman spectra for P25 and its composites with CNTs

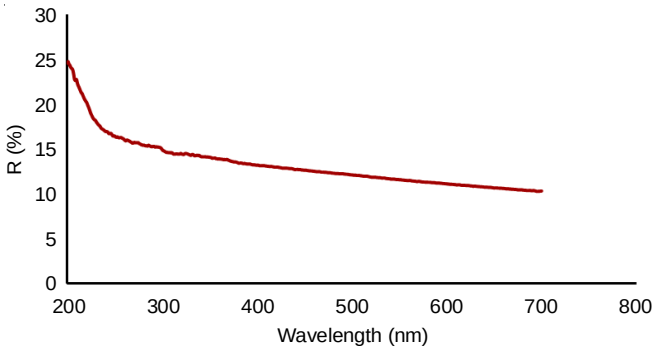

Fig. 4. UV-Vis diffuse reflectance spectra of the synthesized CNTs

Raman bands for P25/CNT composites were slightly broadened compared to pure P25. This broadening of the peak corresponds to a decrease in the average crystallite size [29,30]. The changes in peak broadening are minor, since the CNTs ratios utilized in this study are quite modest.

UV-visible-DRS: Diffuse reflectance spectra of P25, CNTs and P25/CNTs are shown in Figs. 4 and 5. The inclusion of CNTs causes the composite material to absorb from 400 to 800 nm and the absorption even covers the entire visible region. Furthermore, the absorption edge of P25/CNTs nanocomposites exhibits a considerable red shift to higher wavelength, which might be attributed to the electrical interaction between CNT and P25 [31]. As a result, the P25/CNTs composites should have outstanding photocatalytic activity that may be seen. The composites exhibit strong absorption capabilities not only in the ultraviolet but also in visible light, which is important for exploitation and utilization of solar energy resources in solar cell [32].

The diffuse reflectance UV-vis spectra of different samples were measured and expressed in terms of Kubelka-Munk

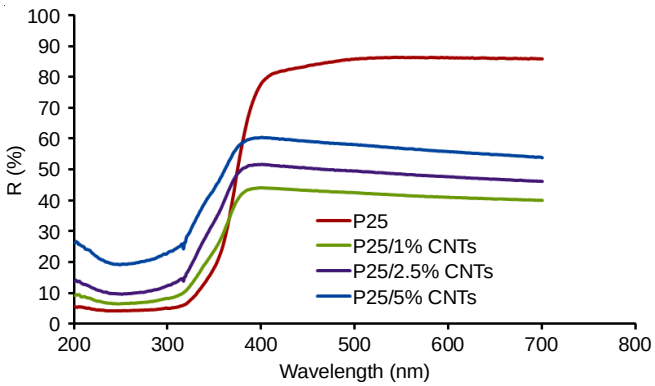

Fig. 5. UV-Vis diffuse reflectance spectra for P25 and its composites with CNTs

equivalent absorption units (Fig. 6). The absorption edges were determined using the following equation once the band gaps have been anticipated:

$$E_g = \frac{1239.8}{\lambda} \quad (2)$$

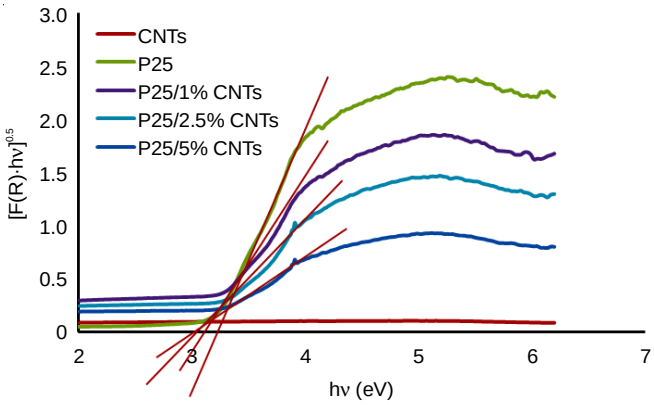

Fig. 6. Kubelka-Munk curves for estimating band gap of the synthesized CNTs and P25/CNTs composites

where λ is the optical absorption edge (nm) and E_g is the band gap (eV). Table-2 shows the band gaps and absorption edges of synthesized samples.

TABLE-2
THE BAND GAPS AND ADSORPTION EDGES

Absorption edge (nm)	Band gap (eV)	Sample
P25	3.22	385.030
1% CNTs + P25	3.10	399.935
2.5% CNTs + P25	3.00	413.266
5% CNTs + P25	2.95	420.271

The band gap values for P25 and synthesized P25/CNTs nanocomposite were 3.22, 3.1, 3 and 2.95 eV, respectively. Reducing band gap energy involves the low energy to accelerate electron excitation from the valance band to the conducting band, resulting in more electron/positive hole pairs and improving the photocatalytic process [33,34]. However, the surface area and density of adsorption active sites influence the photocatalytic reaction as well as the band gap energy value. The small optical differences were observed, which could be due to the formation of CNTs within the pores of P25 NRs and on their surfaces, results in the limitation of the interaction between incident light and P25 as an active component for light. However, this outcomes favours in a significant increase in specific surface area and the presence of the numerous active adsorption sites, which is expected to improve the efficiency of photocatalytic reaction.

SEM studies: The images of P25/CNTs preserve one-dimensional nanostructure of the CNTs (Fig. 7). The coarsening of CNTs surfaces indicates the presence of a P25 coating surface of CNTs. However, the presence of agglomerated particles is not under control during the synthesis procedure and weight fractions of primary materials affect the amount of coated and aggregated P25. From these images, it also can be seen that for both tube for CNTs and the particles of the P25/CNTs composite. The SEM images of nanocomposite refers that the CNTs are homogenously distributed throughout the P25 matrix with an obvious agglomeration of the P25 particles. It is noticed from these images that an average diameter of carbon nanotubes increased slightly as a result of the accumulation of P25 nanoparticles on its surface, with a small increase also in the particle size of the composites, some of which are very close to their crystallite size estimated from XRD diffraction measurements by applying Scherer's equation.

Fabrication of dye-sensitized solar cell: The solar cells were fabricated using P25 and its composite with CNTs as the photoelectrode, as well as Pomegranate dye as photocatalysts. The I-V and P-V characteristics of DSSCs are illustrated in Figs. 8 and 9. Table-3 shows the short-circuit current density (J_{sc}), open-circuit voltage (V_{oc}), fill factor ($FF = J_m \times V_m/J_{sc} \times V_{oc}$) and power conversion efficiency (PCE) of all the cells. The short circuit current was determined by the devices' I–V characteristics. Based on P25/Pt, P25, CNTs compsite/Pt. The photovoltaic cells prepared using P25 were more efficient because the highly efficient commercial photocatalyst and the cells prepared from Pt counter electrode were more efficient because Pt is high exchange current density, good catalytic activity and transparency. The P25/CNTs composite is consider the best photoelectrode and more efficient than P25 alone especially in the ratio 1:2.5%. It is noticed that the type of electrode in the same dye has a very important role in improving the efficiency η of the solar cell. It is possible to explain the results of the decrease in the efficiency of cells when increasing the proportion of carbon nanotubes due to the darkness of the cell and the opacity of FTO glass and this would reduce the absorption of light by the dye. Furthermore, the low obtained η value of the fabricated DSSCs is also due to the low intensity (34 mW/cm^2) of light source that was used. For all prepared DSSCs, A = 2.25 cm^2.

From above results it can be noted that when platinum was used as a counter electrode, the efficiency of its cells is higher when the percentages of P25/CNTs composites are higher. This is due to the reason that the carbon nanotubes increased the surface area of the composites, thus increasing its absorption capacity, in addition to the high efficiency of platinum as a counter electrode in solar cells. But the increase in carbon nanotubes to a large percentage could affect the transparency of the solar cell and thus reduce its efficiency. That is why very few percentages were taken from it. As in the previous figures, where the highest efficiency of the cell reaches to 3.679 at the rate of P25, 2.5% CNTs/Pt.

TABLE-3
PHOTO ELECTROCHEMICAL PARAMETERS OF THE DSSCs,
(A) P25/Pt, (B) P25, 1% CNTs/Pt, (C) P25, 2.5% CNTs/Pt, (D) P25, 5% CNTs/Pt

Types of electrodes	I_{sc} (mA)	V_{oc} (V)	J_{max} (mA)	V_{max} (V)	P_{max}	FF (%)	η (%)
A	8.67	0.590	6.49	0.349	2.265	0.443	2.962
B	8.67	0.600	6.50	0.349	2.268	0.439	2.985
C	8.92	0.715	6.95	0.405	2.814	0.441	3.679
D	8.22	0.620	6.10	0.425	2.592	0.508	3.384

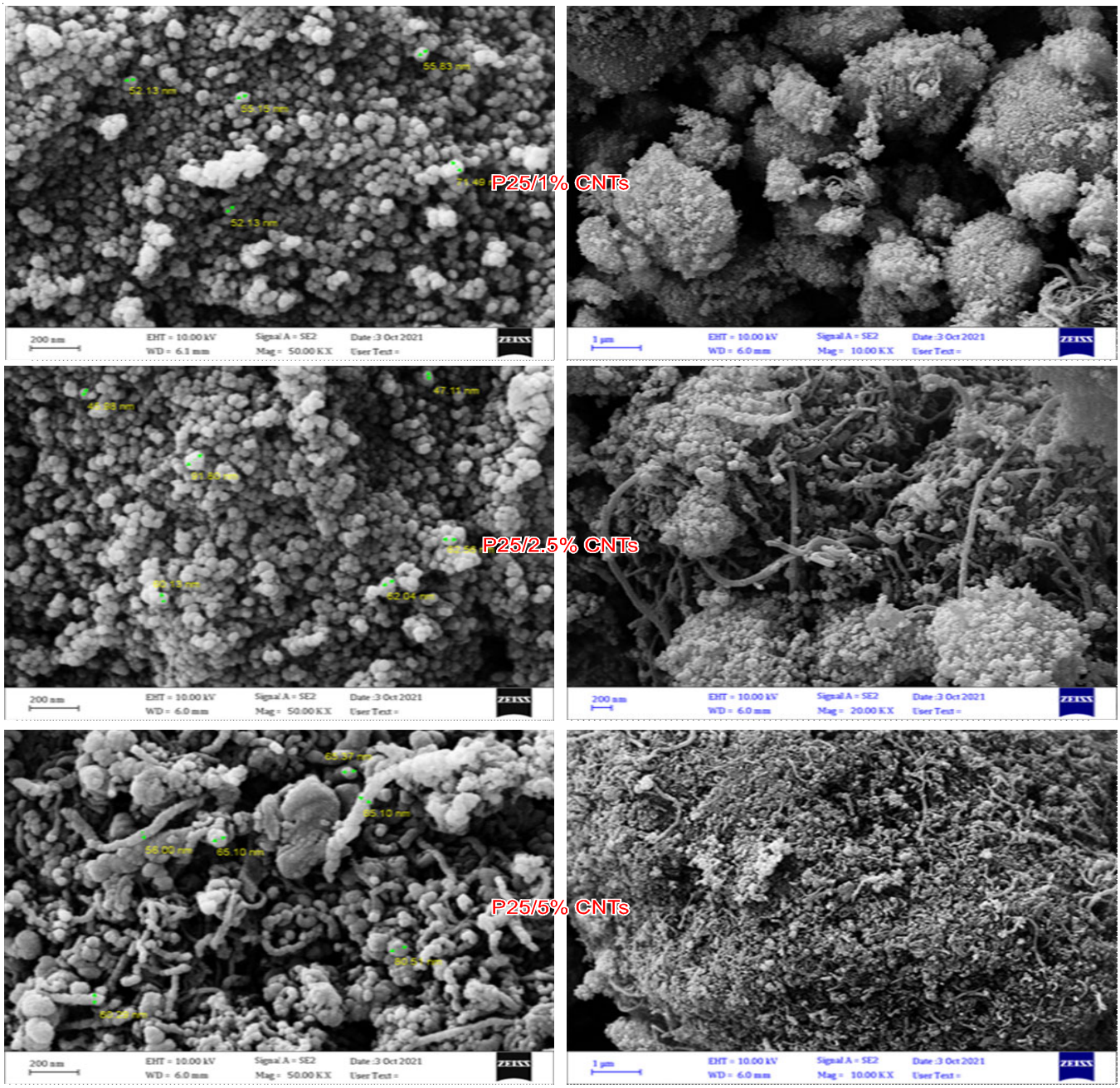

Fig. 7. SEM images for P25/CNTs composites

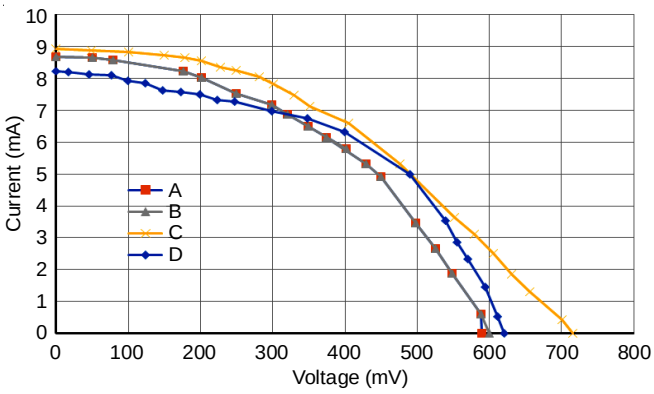

Fig. 8. I-V characteristics of prepared DSSCs, (A) P25/Pt, (B) P25, 1% CNTs/Pt, (C) P25, 2.5% CNTs/Pt (D) P25, 5% CNTs/Pt

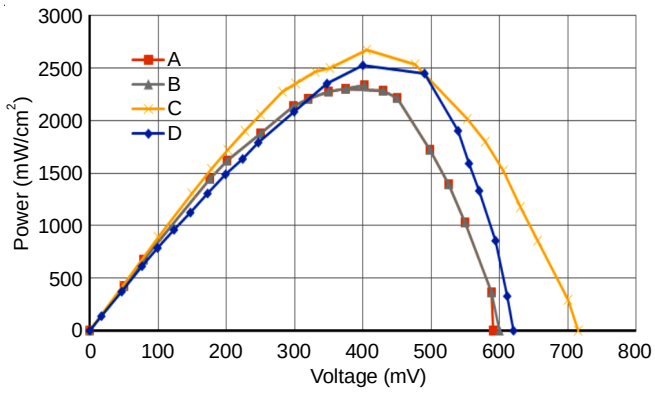

Fig. 9. P-V characteristics of prepared DSSCs, (A) P25/Pt, (B) P25, 1% CNTs/Pt, (C) P25, 2.5% CNTs/Pt, (D) P25, 5% CNTs/Pt

Conclusion

An enhanced efficiency of the prepared dye sensitized solar cell (DSSC) by using Degussa (Evonik) P25 with carbon nanotubes (CNTs) composites as the photoanode electrode instead of using TiO_2 alone were prepared in different ratios and these composites materials were utilized in fabrication of DSSCs as an active photoanode. The conversion efficiency for these DSSCs with photoanode of P25 and P25/CNTs composites were 2.962% and 3.679%, respectively.

CONFLICT OF INTEREST

The authors declare that there is no conflict of interests regarding the publication of this article.

REFERENCES

1. B. O'Regan and M. Grätzel, *Nature*, **353**, 737 (1991); https://doi.org/10.1038/353737a0
2. M. Grätzel, *Prog. Photovolt. Res. Appl.*, **8**, 171 (2000); https://doi.org/10.1002/(SICI)1099-159X(200001/02)8:1<171::AID-PIP300>3.0.CO;2-U
3. Y. Hu, A. Abate, Y. Cao, A. Ivaturi, S.M. Zakeeruddin, M. Grätzel and N. Robertson, *J. Phys. Chem. C*, **120**, 15027 (2016); https://doi.org/10.1021/acs.jpcc.6b03610
4. I.P. Liu, W.N. Hung, H. Teng, S. Venkatesan, J.C. Lin and Y.L. Lee, *J. Mater. Chem. A Mater. Energy Sustain.*, **5**, 9190 (2017); https://doi.org/10.1039/C7TA01341H
5. S.M. Gupta and M. Tripathi, *Chin. Sci. Bull.*, **56**, 1639 (2011); https://doi.org/10.1007/s11434-011-4476-1
6. Q. Huaulme, L. Cabau and R. Demadrille, *Chem*, **4**, 2267 (2018); https://doi.org/10.1016/j.chempr.2018.09.020
7. M. Zi, M. Zhu, L. Chen, H. Wei, X. Yang and B. Cao, *Ceram. Int.*, **40**, 7965 (2014); https://doi.org/10.1016/j.ceramint.2013.12.146
8. L. Wei, P. Wang, Y. Yang, Z. Zhan, Y. Dong, W. Song and R. Fan, *Inorg. Chem. Front.*, **5**, 54 (2018); https://doi.org/10.1039/C7QI00503B
9. M. Pelaez, N.T. Nolan, S.C. Pillai, M.K. Seery, P. Falaras, A.G. Kontos, P.S.M. Dunlop, J.W.J. Hamilton, J.A. Byrne, K. O'Shea, M.H. Entezari and D.D. Dionysiou, *Appl. Catal. B*, **125**, 331 (2012); https://doi.org/10.1016/j.apcatb.2012.05.036
10. V.M. Ramakrishnan, M. Natarajan, A. Santhanam, V. Asokan and D. Velauthapillai, *Mater. Res. Bull.*, **97**, 351 (2018); https://doi.org/10.1016/j.materresbull.2017.09.017
11. Z.S. Wang, H. Kawauchi, T. Kashima and H. Arakawa, *Coord. Chem. Rev.*, **248**, 1381 (2004); https://doi.org/10.1016/j.ccr.2004.03.006
12. Y.K. Hwang, S.S. Park, J.H. Lim, Y.S. Won and S. Huh, *J. Nanosci. Nanotechnol.*, **13**, 2255 (2013); https://doi.org/10.1166/jnn.2013.6897
13. Z. Zhao, G. Liu, B. Li, L. Guo, C. Fei, Y. Wang, L. Lv, X. Liu, J. Tian and G. Cao, *J. Mater. Chem. A Mater. Energy Sustain.*, **3**, 11320 (2015); https://doi.org/10.1039/C5TA01953B
14. P. Zhao, S. Yao, M. Wang, B. Wang, P. Sun, F. Liu, X. Liang, Y. Sun and G. Lu, *Electrochim. Acta*, **170**, 276 (2015); https://doi.org/10.1016/j.electacta.2015.04.102
15. K.P. Ghoderao, S.N. Jamble and R.B. Kale, *Superlattices Microstruct.*, **124**, 121 (2018); https://doi.org/10.1016/j.spmi.2018.09.038
16. B.R. Koo, H. An and H.J. Ahn, *Ceram. Int.*, **42**, 1666 (2016); https://doi.org/10.1016/j.ceramint.2015.09.120
17. Z. Hou, W. Que, J. Ren, Y. Xing, H.A. Javed, T. Zhou and L.B. Kong, *Ceram. Int.*, **41**, S719 (2015); https://doi.org/10.1016/j.ceramint.2015.03.186
18. J. Qu and C. Lai, *J. Nanomater.*, **2013**, 762730 (2013); https://doi.org/10.1155/2013/762730
19. M. Adachi, Y. Murata, J. Takao, J. Jiu, M. Sakamoto and F. Wang, *J. Am. Chem. Soc.*, **126**, 14943 (2004); https://doi.org/10.1021/ja048068s
20. H. Park, Y. Park, W. Kim and W. Choi, *J. Photochem. Photobiol. Photochem. Rev.*, **15**, 1 (2013); https://doi.org/10.1016/j.jphotochemrev.2012.10.001
21. A.H. Hammadi, A.M. Jasim, F.H. Abdulrazzak, A. Al-Sammarraie, Y. Cherifi, R. Boukherroub and F.H. Hussein, *Materials*, **13**, 2342 (2020); https://doi.org/10.3390/ma13102342
22. A.H. Hammadi, F.H. Abdulrazzak, A.J. Atiyah and F.H. Hussein, *Org. Med. Chem. Int. J.*, **6**, 555699 (2018); https://doi.org/10.19080/OMCIJ.2018.06.555699
23. X. Liu, G. Xiao, W. Chen, Y. Xu and J. Wu, *J. Biomed. Biotechnol.*, **2004**, 326 (2004); https://doi.org/10.1155/S1110724304403052
24. M.Q. Lokman, S. Shafie, S. Shaban, F. Ahmad, H. Jaafar, R.M. Rosnan, H. Yahaya and S.S. Abdullah, *Materials*, **12**, 2111 (2019); https://doi.org/10.3390/ma12132111
25. G. Yue, R. Cheng, X. Gao, L. Fan, Y. Mao, Y. Gao and F. Tan, *Nanoscale Res. Lett.*, **15**, 179 (2020); https://doi.org/10.1186/s11671-020-03410-0
26. M. Halka, S. Smoleń, I. Ledwozyw-Smoleń and W. Sady, *J. Plant Growth Regul.*, **39**, 282 (2020); https://doi.org/10.1007/s00344-019-09981-2
27. O. Carp, C.L. Huisman and A. Reller, *Prog. Solid State Chem.*, **32**, 33 (2004); https://doi.org/10.1016/j.progsolidstchem.2004.08.001
28. N. Bouazza, M. Ouzzine, M.A. Lillo-Ródenas, D. Eder and A. Linares-Solano, *Appl. Catal. B*, **92**, 377 (2009); https://doi.org/10.1016/j.apcatb.2009.08.017
29. G. Liu, X. Yan, Z. Chen, X. Wang, L. Wang, G.Q. Lu and H.M. Cheng, *J. Mater. Chem.*, **19**, 6590 (2009); https://doi.org/10.1039/b902666e
30. R. Saito, G. Dresselhaus and M.S. Dresselhaus, *Phys. Rev. B Condens. Matter Mater. Phys.*, **61**, 2981 (2000); https://doi.org/10.1103/PhysRevB.61.2981
31. M. Ding, D.C. Sorescu and A. Star, *J. Am. Chem. Soc.*, **135**, 9015 (2013); https://doi.org/10.1021/ja402887v
32. H. Eskandarloo, A. Badiei, M.A. Behnajady and G.M. Ziarani, *Chem. Eng. J.*, **270**, 158 (2015); https://doi.org/10.1016/j.cej.2015.01.117
33. M. Shaban, M.R. Abukhadra and A. Hamd, *Clean Technol. Environ. Policy*, **20**, 13 (2018); https://doi.org/10.1007/s10098-017-1447-5
34. M. Shaban, M.R. Abukhadra, A. Hamd, R.R. Amin and A. Abdel Khalek, *J. Environ. Manage.*, **204**, 189 (2017); https://doi.org/10.1016/j.jenvman.2017.08.048